Commun. Comput. Phys.
doi: 10.4208/cicp.191114.270315a

Vol. **18**, No. 3, pp. 707-722
September 2015

Direct Numerical Simulation of an Open-Cell Metallic Foam through Lattice Boltzmann Method

Daniele Chiappini[1,*], Gino Bella[2], Alessio Festuccia[2] and Alessandro Simoncini[2]

[1] *University Niccoló Cusano - Department of Mechanical Engineering, Via don Carlo Gnocchi 3, 00166 Rome (RM), Italy.*
[2] *University of Rome Tor Vergata - Department of Mechanical Engineering, Via del Politecnico 1, 00133 Rome (RM), Italy.*

Received 19 November 2014; Accepted (in revised version) 27 March 2015

Abstract. In this paper Lattice Boltzmann Method (LBM) has been used in order to perform Direct Numerical Simulation (DNS) for porous media analysis. Among the different configurations of porous media, open cell metallic foams are gaining a key role for a large number of applications, like heat exchangers for high performance cars or aeronautic components as well. Their structure allows improving heat transfer process with fruitful advantages for packaging issues and size reduction. In order to better understand metallic foam capabilities, a random sphere generation code has been implemented and fluid-dynamic simulations have been carried out by means of a kinetic approach. After having defined a computational domain the Reynolds number influence has been studied with the aim of characterizing both pressure drop and friction factor throughout a finite foam volume. In order to validate the proposed model, a comparison analysis with experimental data has been carried out too.

PACS: 47.11.-j, 47.11.Qr, 47.15.Rq, 47.56.+r

Key words: LBM, DNS, porous media simulation, metallic foam characterization.

1 Introduction

Metallic foam components are gaining an always rising up relevance and their applications in a large number of engineering processes are occurring. For example, porous media, like metallic foams, are nowadays applied to heat exchangers both for industrial or electronic devices [1–3]. Then a precise and accurate knowledge about fluid-dynamic

*Corresponding author. *Email addresses:* daniele.chiappini@unicusano.it (D. Chiappini), bella@uniroma2.it (G. Bella), alessio.festuccia@gmail.com (A. Festuccia), alessandrosimoncini@hotmail.it (A. Simoncini)

 ©2015 Global-Science Press

https://doi.org/10.4208/cicp.191114.270315a Published online by Cambridge University Press

phenomena which take place into a porous medium is becoming really helpful for future developments. Being the metallic foam randomly organized, the mathematical solution of involved continuum equations is a challenging issue to be solved, [2]. Many authors [1,4–8] used a simplified cell derived from the Lord Kelvin one, commonly named tetrakaidecahedron. The main disadvantage of this approach is the lack of randomness due to the intrinsic cell structure. On the other hand, starting from the images obtained by means of micro-tomography, an alternative approach, based on random packing distribution, has been proposed [9,10], with apparent benefits in terms of mesh generation. Then, the aim of this paper is to couple the latter approach with a three dimensional Lattice Boltzmann scheme.

During last decades, in fact, Lattice Boltzmann Method (LBM) has gained an always rising importance over numerical simulation methods due to its simplicity on implementation and accuracy in solving fluid-dynamics problems in the range of small Knudsen numbers [11–13]. In order to speed up simulation, an optimized parallel version of the source code has been developed with significant benefits in computational time. Lattice Boltzmann Equation (LBE) may be used in order to solve a wide range of cases where the fluid compressibility may be neglected. As already pointed out by [14,15] Lattice Boltzmann Method may be applied for a large number of applications which involve multiphase flows too. More precisely, in this paper, the attention is addressed to the definition of an alternative approach for metallic foam simulation. The main advantage in using a LBM is to perform a direct numerical simulation and to locally solve involved equations in a large number of grid points but with relatively low computational requirements also for complex geometries like porous media. More specifically, starting from a random sphere packing approach, the laminar flow behaviour of a metallic foam is deeply analysed, by varying Reynolds number, porosity level and grid definition as well. The goal is to find a correlation between numerical model and experimental results, presented by [10] and in the same time to define Ergun equations coefficients, [16], for the specific test case. After model validation, a sensitivity analysis to geometric parameters and material properties is carried out with the aim of predicting the fluid-dynamic behaviour of a generic metallic foam. This approach allows determining a foam characteristics at the beginning of the design phase with obvious advantages during project development.

2 The Lattice Boltzmann Method

The LBM represents a useful alternative to standard Navier-Stokes models. Starting from a microscopic kinetic approach for fluid flow solution, it mathematically describes movements and interactions of the small particles that constitute the flow. The LBM is based [11–13] on a discrete decomposition of Boltzmann equation into velocity space, which allows writing the discrete form of the Boltzmann equation for a set of speeds as

https://doi.org/10.4208/cicp.191114.270315a Published online by Cambridge University Press

in the following equation:

$$\frac{\partial f_\alpha(\mathbf{x},t)}{\partial t}+\mathbf{c}_\alpha\nabla f_\alpha(\mathbf{x},t)=-\frac{1}{\tau}\left[f_\alpha(\mathbf{x},t)-f_\alpha^{eq}(\mathbf{x},t)\right], \tag{2.1}$$

where $f(\mathbf{x},t)$ is the particle distribution function which gives information about finding a particle at position $\mathbf{x}$ at time t with a discrete velocity $\mathbf{c}$ along one of the allowed directions $\mathbf{c}_\alpha$ (usually 9 for a 2D simulation and 19 for a 3D simulation), [13, 17, 18]. In this paper a $D3Q19$ stencil is used for flow discretization coupled with a uniform Cartesian lattice. The approach used is a single-relaxation time τ to the local equilibrium f_{eq}, where the local equilibrium is a function of the macroscopic flow variables according to the following equation (2.2):

$$f_\alpha^{eq}(\mathbf{x},t)=w_\alpha\rho(\mathbf{x},t)\left[\frac{\mathbf{c}_\alpha\cdot\mathbf{u}(\mathbf{x},t)}{c_s^2}+\frac{\left[\mathbf{c}_\alpha\cdot\mathbf{u}(\mathbf{x},t)\right]^2}{2c_s^4}-\frac{\left[\mathbf{u}(\mathbf{x},t)\cdot\mathbf{u}(\mathbf{x},t)\right]}{2c_s^2}\right] \tag{2.2}$$

being w_α a set of weights normalized to unity. $\rho(\mathbf{x},t)$ and $\mathbf{u}(\mathbf{x},t)$ are respectively global density and speed and c_s is the lattice speed of sound, [19].

Solving with an explicit approach equation (2.1) leads to the following discrete form:

$$\begin{aligned}\Delta_\alpha f_\alpha(\mathbf{x},t)&=f_\alpha(\mathbf{x}+\mathbf{c}_\alpha\Delta t,t+\Delta t)-f_\alpha(\mathbf{x},t)\\&=-\frac{\Delta t}{\tau}\left[f_\alpha(\mathbf{x},t)-f_\alpha^{eq}(\mathbf{x},t)\right],\end{aligned} \tag{2.3}$$

which may be explicitly solved every time-step. In conclusion the 0^{th} and the 1^{st} population momentum allow evaluating fluid density and speed:

$$\rho(\mathbf{x},t)=\sum_{\alpha=0}^{N_{pop}-1}f_\alpha(\mathbf{x},t), \tag{2.4a}$$

$$\rho\mathbf{u}(\mathbf{x},t)=\sum_{\alpha=0}^{N_{pop}-1}\mathbf{c}_\alpha f_\alpha(\mathbf{x},t), \tag{2.4b}$$

where N_{pop} denotes the number of discrete velocities (or populations). For small Knudsen numbers and small Mach numbers (*fluid near the incompressibility limit*), it can be shown [11] through the Chapman-Enskog expansion that the above formulation recovers the dynamic behaviour of an ideal fluid with pressure $P=\rho c_s^2$ and kinematic viscosity $\nu=c_s^2(\tau-\Delta t/2)$.

From previous equations it is obvious how this method is explicitly solvable with small memory occupation.

3 From global to LBM quantities

As previously mentioned LB methods reconstruct global quantities by means of a local distribution function which is solved through a uniform Cartesian lattice. Thus, passage

https://doi.org/10.4208/cicp.191114.270315a Published online by Cambridge University Press

from global to local quantities is mandatory. Starting, for example, from a real mean pore diameter D_{Phys} and imposing the number of lattice grid-points which represent the pore diameter into the dimensionless domain $D_{l.u.}$, the length conversion factor is:

$$S_l = \frac{D_{Phys}}{D_{l.u.}} \left[\frac{\text{m}}{\text{l.u.}}\right]. \tag{3.1}$$

This mandatory passage gives the immediate feeling how to convert physical quantities to LB ones.

With a similar procedure, starting from a dimensional analysis of the kinematic viscosity, it is trivial to get that the international system units are m^2/s. Then, via combining the viscosity ratio (physical over dimensionless) with the length conversion factor above mentioned, a time conversion factor may be defined too. These simple considerations lead to the following equation:

$$S_t = \frac{\nu_{l.u.}}{\nu_{Phys}} S_l^2 \left[\frac{\text{s}}{\text{l.u.}}\right]. \tag{3.2}$$

By means of kinetic viscosity, which may be assumed constant into the range of small Knudsen numbers, it is possible to associate a LB time-step to the real time evolution.

The last parameter, needed to fully characterize the system, is the mass conversion factor, which may be derived starting from density ratio (physical over dimensionless) and the length conversion factor previously defined:

$$S_m = \frac{\rho_{Phys}}{\rho_{l.u.}} S_l^3 \left[\frac{\text{kg}}{\text{l.u.}}\right]. \tag{3.3}$$

By means of S_l, S_t and S_m, introduced in Eqs. (3.1), (3.2) and (3.3), it is possible to describe all physical quantities which may be analysed. More specifically, pressure drop per unit length may be evaluated as follows:

$$P_{Phys} = P_{l.u.} \frac{S_m}{S_l \cdot S_t^2}. \tag{3.4}$$

The passage from LB pressure drop to physical one is fundamental in order to correlate simulation results to experimental ones.

4 The Ergun equation

As pointed out before, the aim of this work is to numerically determine the pressure drop of an open-cell metallic foam as a function of Reynolds number in the region of laminar flow. Ergun equation [16] represents a well consolidated approach used to determine porous media pressure drop as a function of Reynolds number. The governing equation is equal to:

$$\frac{\Delta P}{L} = \frac{\rho}{D_P} \frac{1-\epsilon}{\epsilon^3} \left(A \frac{1-\epsilon}{Re} + B \right) c^2, \tag{4.1}$$

https://doi.org/10.4208/cicp.191114.270315a Published online by Cambridge University Press

where:

- A and B represent unknown coefficients which may be evaluated starting from experiments/simulations results;
- ρ is the fluid density;
- ϵ the porosity of porous medium;
- D_P the equivalent particle diameter;
- Re is the particle Reynolds number which will be defined in the following sections, Eq. (6.1);
- c is the imposed inlet fluid velocity.

Having a consistent set of data, the above mentioned Ergun coefficients may be evaluated [10, 20, 21], and the pressure drop evolution as a function of pore Reynolds number reconstructed as well. In this work, the coefficients A and B have been derived using numerical pressure drops coupled with least squares minimization method for data fitting.

In order to solve the Ergun equation the equivalent particle diameter D_P has to be defined too. This is a function both of the mean pore diameter d and of the porosity ϵ, as reported in the following equation:

$$D_P = \frac{3}{2}\frac{1-\epsilon}{\epsilon}d. \tag{4.2}$$

As previously stated, having a limited set of available data, the evaluation of A and B coefficients is possible only via a data fitting technique. After their determination, Eq. (4.1) may be use in order to predict metallic foam behaviour in the whole range of interesting Reynolds numbers not covered by the experimental/simulation campaign. Performance results of porous media have often been analysed in terms of friction factor ϕ_k, which is, of course, function of the pressure drop itself:

$$\phi_k = \frac{\Delta P}{L}\frac{D_P}{\rho c^2}\frac{\epsilon^3}{1-\epsilon}. \tag{4.3}$$

By combining Ergun equation (4.1) with friction factor (4.3), its alternative expression as a function of A and B parameters and of pore Reynolds number may be derived:

$$\phi_k = A\frac{1-\epsilon}{Re} + B. \tag{4.4}$$

5 Porous media grid generation

Different approaches may be used for open-cell metallic foam simulations. Some authors model the porous cell using a complex geometric structure like the tetrakaidecahedron

https://doi.org/10.4208/cicp.191114.270315a Published online by Cambridge University Press

[6,7]. The limit of this approach is that the random porous structure is transformed to a regular grid with packed reference elements. On the other hand, other authors propose a random grid generation in order to match information from micro-tomography or X-ray pictures, [9,22]. In this paper the latter approach is used and a specific code for grid generation has been developed.

The proposed method starts from spheres randomly generated inside the control volume. In order to represent porous media, the volume inside every sphere is representative of the vacuum area, while all the volume outside the sphere itself is referred to metallic structure. Highly porous media, which are the main focus of the present work, are characterized by high vacuum volumes compared to the metallic ones. Then, a certain amount of spheres has to be randomly distributed over space in order to fulfil test case requirements in terms of porosity and pore per inch distribution (PPI). Basically, two different probabilistic distributions have been used respectively for coordination number and spheres' radii [22]. More specifically, the coordination number (CN), which represents the number of contact spheres with the target one, has been described through a β distribution, while the pores' radius has been represented through a standard distribution centred around the mean pore diameter imposed by input. In fact, the mean pore diameter is strictly related to the pore per inch (PPI) information which is a physical material property. In the following a short overview of the grid generation code is presented.

A first sphere is randomly generated into the control volume with a random radius and a random coordination number. Its initial position is located nearly the center of the control volume. Subsequently, a number of spheres equal to the coordination number of the target sphere is generated. There are, of course, some constraints which have to be respected while spheres are added:

- The new sphere added into domain has to guarantee a minimum contact with the target sphere. The check is made through centre position and radius:

$$\sqrt{\left(x_{C,i}-x_{C,target}\right)^2+\left(y_{C,i}-y_{C,target}\right)^2+\left(z_{C,i}-z_{C,target}\right)^2}<\left(r_i-r_{target}\right). \tag{5.1}$$

- The maximum interpenetration between the two spheres is ruled by the maximum overlap allowed. In this application the overlap is a percentage of the minimum radius of the two spheres, the target one and the new one. In other words, the maximum interpenetration condition has to be implemented as follows:

$$\begin{aligned}&\sqrt{\left(x_{C,i}-x_{C,target}\right)^2+\left(y_{C,i}-y_{C,target}\right)^2+\left(z_{C,i}-z_{C,target}\right)^2}\\&>\left(r_i-r_{target}-Overlap\cdot r_{\min}\right).\end{aligned} \tag{5.2}$$

- The new sphere has to be totally or partially included into physical domain:

$$\begin{cases}x_{C,i}+r\geq X_0 \;\&\; x_{C,i}-r\leq X_F\\ y_{C,i}+r\geq Y_0 \;\&\; y_{C,i}-r\leq Y_F\\ z_{C,i}+r\geq Z_0 \;\&\; z_{C,i}-r\leq Z_F\end{cases} \tag{5.3}$$

https://doi.org/10.4208/cicp.191114.270315a Published online by Cambridge University Press

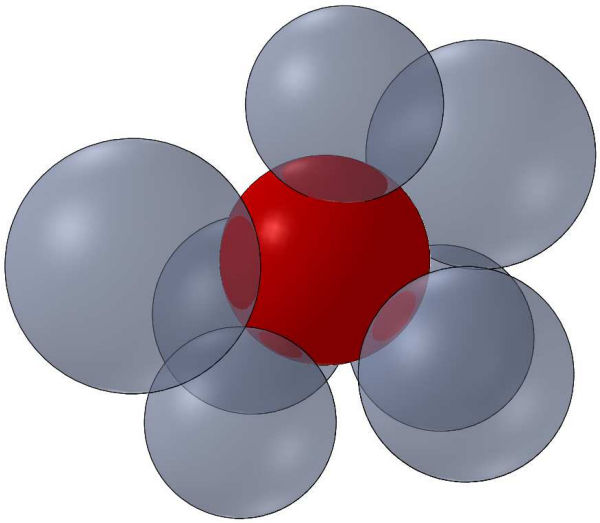


Figure 1: Sketch of a saturated sphere.

While the coordination number for the target sphere is satisfied the above mentioned loop is repeated for all the spheres present into the domain. In Fig. 1 a saturated target sphere (red) is shown.

Of course the procedure is repeated until the control volume is filled and, at the end of grid generation, a porosity check is carried out too. The degree of freedom used to partially rearrange the porosity is the pore radius. The more spheres' radius rises up the more the porosity increases, until reaching the limit condition of a control volume completely filled by air.

6 Model validation

In order to validate the proposed model, a comparison with experimental results is needed. The reference chosen is the set of results presented in [10] for a metallic foam with porosity $\epsilon = 0.955$. The results are compared in terms of friction factor as a function of particle Reynolds number, defined as follows:

$$Re = \frac{cD_P}{\nu}, \tag{6.1}$$

where c is the inlet fluid velocity imposed as a boundary condition. Once fixed both kinematic viscosity and average pore diameter, the inlet fluid velocity may be easily evaluated as a function of pore Reynolds number, using Eq. (6.1). In the following the particle Reynolds number is considered as reference, for sake of brevity it is simply named Re. It is trivial to notice how this Reynolds number is a function of equivalent particle diameter, which takes into account both PPI and porosity information, as reported into Eq. (4.2).

https://doi.org/10.4208/cicp.191114.270315a Published online by Cambridge University Press

All the simulations have been performed in a fluid domain structured as follows:

- inlet buffer ($50\times200\times200$ l.u.);
- porous domain ($200\times200\times200$ l.u.);
- outlet buffer ($50\times200\times200$ l.u.).

The boundary conditions in the above described domain are imposed velocity for inlet section and imposed pressure at outlet one. For all the remaining walls the mid-grid bounce back is considered in order to be second order accurate [11]. Both inlet and outlet buffers are used with the aim of stabilizing fluid flow before and after the porous medium inlet/outlet sections. The metallic porous domain has been treated with a mid-grid bounce back too. Being the minimum pore diameter about 43 l.u., the sphere may be represented through a stepped surface. Of course this simplification is applicable due to the relatively high number of lattice sites used for pore representation which allow reconstructing complex geometries without losing curvature definition and without apparent issues related to method accuracy. Moreover, the minimum pore diameter above mentioned implies a maximum Knudsen number [13], equal to:

$$Kn_{\max}=\frac{\lambda_m}{D_{\min}}=\sqrt{\frac{\pi}{2}}\frac{\tau c_s}{D_{\min}}=0.0169. \tag{6.2}$$

Then the molecular mean free path is definitely smaller than the minimum pore diameter ($\lambda_m \ll D_{\min}$).

After having described the model set-up, the friction factor as a function of Reynolds number for a metallic foam with a porosity equal to $\epsilon=95.5\%$ is presented, as reported in [10]. It has been already pointed out how the friction factor is a function of the pressure drop per unit length and of the porosity itself, (4.3). More specifically a set of simulations for different Reynolds number has been carried out and the out-coming results have been compared with the experimental ones [10]. The comparison of numerical simulation results with an experimental campaign is one of the first steps needed in every model validation and, for the test case under analysis, it is depicted in Fig. 2, where the red line is referred to experimental results provided by [10], and the blue line is representative of the simulation ones.

It is quite apparent how there is a perfect agreement between numerical and experimental results, especially for higher Reynolds numbers, where the friction factor obtained by means of LBM simulations practically overlaps the experimental results. There is only a slight misalignment at really low Reynolds numbers due to almost vanishing pressure drops which occur at low speeds. In the following sections a sensitivity analysis both to mesh definition and porosity level will be performed, in order to analyse their influence on the porous media physical behaviour.

Finally, for Ergun equation definition, both coefficients A and B are evaluated for the simulations results by means of a least squares minimization procedure. The Ergun

https://doi.org/10.4208/cicp.191114.270315a Published online by Cambridge University Press

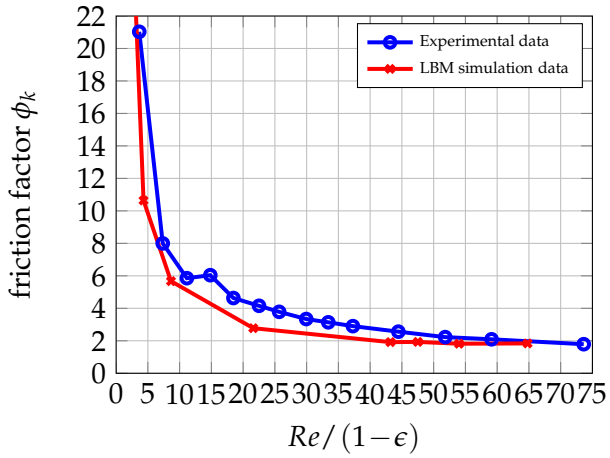


Figure 2: Comparison between experimental results and simulations in terms of friction factor.

coefficient comparison obtained by [10] and evaluated in this work is reported in Table 1. As it can be observed there is a slight misalignment between obtained results and the reference ones. This is basically due to the fact that for low Reynolds number the friction factor from LBM simulation is underestimating the experimental one. Nevertheless, at higher Reynolds number results are completely overlapped.

Table 1: Comparison for Ergun coefficients.

	Experimental [10]	Numerical LBM
A	77.85	43.18
B	0.77	0.90

7 Sensitivity analysis to mesh definition

As may be observed from Fig. 2 there is a slight misalignment between experimental data and numerical results at low Reynolds numbers. In order to better understand this deviation, a sensitivity analysis to grid dimension has been carried out too. More specifically, the influence of the number of lattice sites used for describing the pore diameter has been analysed. Starting from mesh definition used in the model validation section, a coarser and a finer grids have been used during simulations in the region of really low Reynolds numbers. A detail of lattice units used for pore diameter description is reported in Table 2.

Table 2: Lattice units for pore diameter description in the sensitivity grid analysis.

	Std. (Fig. 2)	Coarse	Fine
D [l.u.]	55	25	80

https://doi.org/10.4208/cicp.191114.270315a Published online by Cambridge University Press

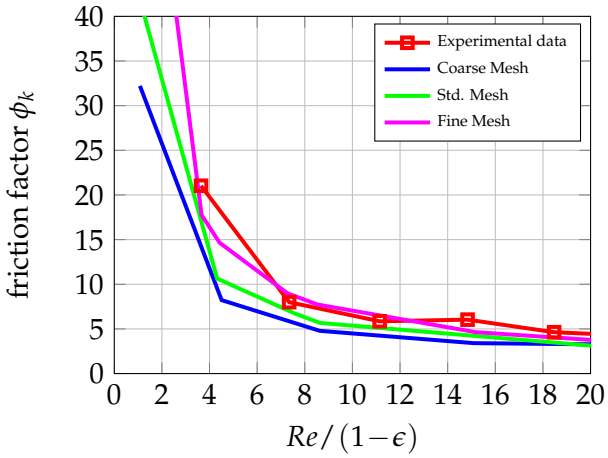


Figure 3: Friction factor as a function of mesh definition.

The results of mesh analysis are depicted in Fig. 3. Again, it is important to evaluate the Knudsen number for the three considered meshes in order to avoid any departure from continuum behaviour (slip layer formation – departure from equilibrium distribution) [11, 13]. The results obtained are briefly reported into Table 3 in terms of minimum pore diameters and corresponding maximum Knudsen numbers. As can be easily observed, the coarser the grid is, the higher the Knudsen number becomes. Nevertheless, with the smallest pore diameter considered, the molecular mean free path is still two orders of magnitude shorter than the characteristic length.

Table 3: Minimum pore diameter and maximum Knudsen number in the sensitivity grid analysis.

	Std. (Fig. 2)	Coarse	Fine
$D_{\min}$ [l.u.]	43	14	65
$Kn_{\max}$	0.0169	0.0503	0.0112

As it may be observed with the finest grid there is a perfect agreement between results also at really low Reynolds numbers. This is an expected result, but it is really important to point out the improvements in terms of deviation from experimental data. Thus, in order to quantify the misalignment, the relative error, defined as follows, is evaluated as a function of particle Reynolds number:

$$\eta = \frac{\left|\phi_k^{(i)} - \phi_k^{exp}\right|}{\phi_k^{exp}}, \tag{7.1}$$

where $\phi_k^{(i)}$ represents the simulation result in terms of friction factor and ϕ_k^{exp} is the corresponding experimental result at the same particle Reynolds number. The error function is summarized in Table 4. As it may be observed, the finer the mesh is, the smaller the

https://doi.org/10.4208/cicp.191114.270315a Published online by Cambridge University Press

Table 4: Relative error as a function of particle Reynolds number.

$Re/(1-\epsilon)$	Coarse Mesh	Std. Mesh	Fine Mesh
3.64	32.12 %	18.46 %	13.19 %
7.34	26.73 %	12.30 %	11.51 %
11.14	27.37 %	12.67 %	11.29 %

relative error in comparison with experimental data becomes. It is interesting to notice how, passing from the coarse to the fine mesh, the relative error at low Reynolds numbers is practically reduced by a factor 2.5. Of course, this effect is less apparent, but always noticeable, passing from standard to fine mesh.

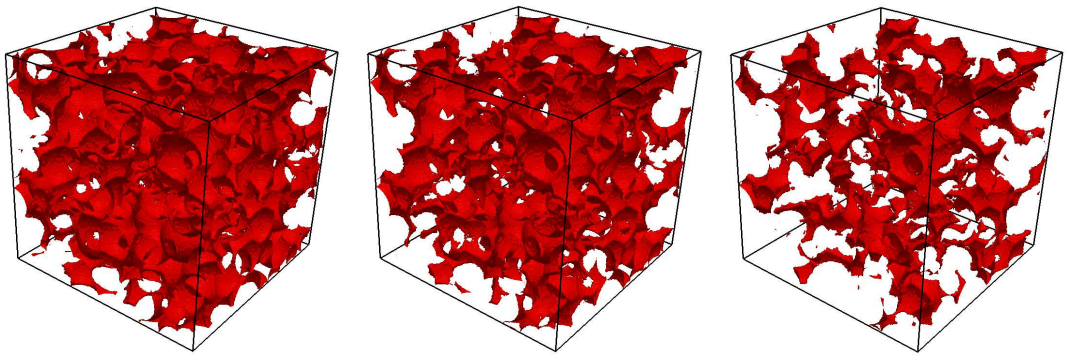
After having pointed out the influence of mesh definition, the influence of porosity level is analysed in the following section.

8 Sensitivity analysis to porosity

In order to better point out the capabilities of the developed model, a sensitivity analysis to porosity influence is carried out in this section. More precisely, three different porosity levels, which may be representative of a real application, have been considered:

1. $\epsilon = 85.0\%$;
2. $\epsilon = 90.0\%$;
3. $\epsilon = 95.5\%$.

For these three porosity levels, three different meshes have been generated, as reported in Fig. 4. As it may be easily observed from Fig. 4, the higher the porosity is, the more "empty" fluid cells are present.



(a) 85% porosity (b) 90% porosity (c) 95.5% porosity

Figure 4: Different meshes comparison with porosity variation.

https://doi.org/10.4208/cicp.191114.270315a Published online by Cambridge University Press

The porosity level, of course, influences the grid definition and the pore diameter distribution itself. Thus, before presenting obtained results, it is useful to report a summarizing table with the minimum pore diameter reached and the maximum Knudsen number (Table 5). Again, the considered meshes allow reaching relatively low Knudsen numbers with well know benefits for simulation.

Table 5: Minimum pore diameter and maximum Knudsen number in the porosity sensitivity analysis.

	$\epsilon=85.0\%$	$\epsilon=90.0\%$	$\epsilon=95.5\%$
$D_{\min}$ [l.u.]	36	33	42
$Kn_{\max}$	0.0202	0.0213	0.0169

For all the test cases considered a set of simulations at different particle Reynolds numbers have been carried out. By the way, all of them are included into the laminar flow regime. The results are compared in terms of delta pressure per unit length and friction factor too. Moreover, for all of them, the Ergun equation is derived in order to be able to predict porous medium behaviour at higher Reynolds numbers. In Fig. 5, the results in terms of friction factor are reported. As it can be observed, the porosity level strongly influences the friction factor which rises up for lower values of ϵ. The shift between curves is clear at higher particle Reynolds numbers where the slope is practically horizontal. For really low particle Reynolds numbers the difference is always present, but it may be affected by the numerical errors which might rise up for really low flow speeds. In these conditions, in fact, a small error on pressure drop evaluation may lead to a significant deviation in terms of friction factor.

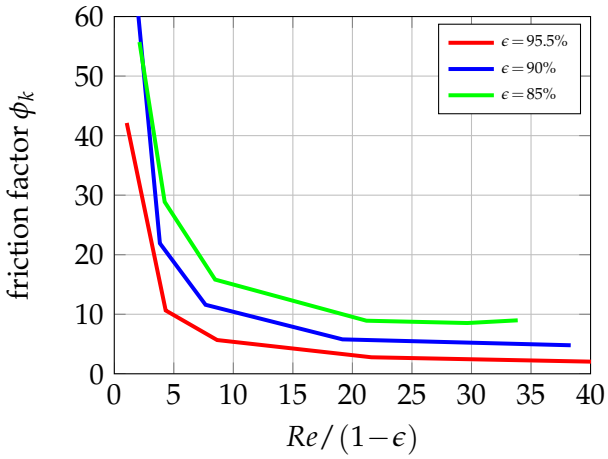


Figure 5: Friction factor as a function of porosity.

Similarly, the pressure drop per unit length may be depicted too, as reported into the next figure where it is a function of particle Reynolds number Re, but it is somehow

https://doi.org/10.4208/cicp.191114.270315a Published online by Cambridge University Press

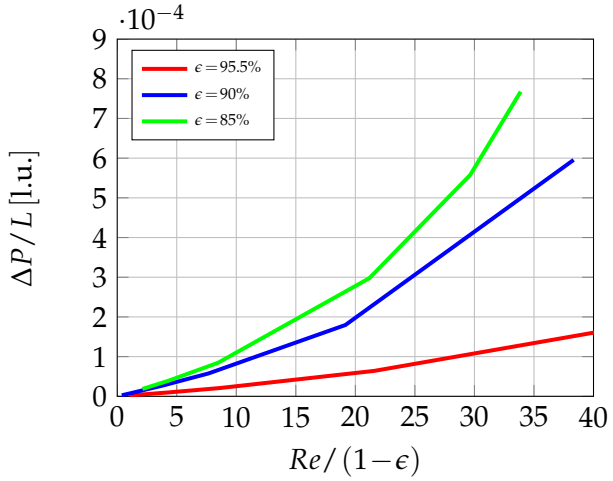


Figure 6: Pressure drop in lattice units as a function of porosity.

made dimensionless by means of the porosity. By this way it is possible to compare in the same graph the results obtained for different porosity levels and, thus, for different computational grids. As already discussed for friction factor, misalignment among different porosity values are quite apparent. The gap between the porosities of 90% and 95.5% is definitely bigger than the one observed for 85% and 90%. This unbalance is not noticeable looking at friction factor curves, as reported in Fig. 5.

Finally, Ergun equation coefficients [16], may be derived for the three configurations analysed. In Table 6, the coefficients derived by means of a least squares minimization are reported for all the porosities considered. Both A and B coefficients becomes smaller when the porosity rises up. This is basically due to the fact that, looking at Fig. 6, the curves for higher porosities are *flatter* than the ones referred to lower ones, as a consequence of a smaller flow resistance. The conclusion is that the bigger A coefficient is, the steeper the pressure curve is. In other words, A coefficient represents a kind of "slope" for pressure drop curve. On the other hand the B coefficient represents a shifting parameter for friction factor curve. In fact, for higher porosity, where a lower friction factor is expected a smaller B coefficient is derived too. Thus, the B coefficient is the asymptote for friction factor at really high Reynolds numbers.

Table 6: Ergun coefficients as a function of porosity.

	$\epsilon = 85.0\%$	$\epsilon = 90.0\%$	$\epsilon = 95.5\%$
A	107.30	67.25	43.18
B	4.39	2.71	0.90

Finally, after having evaluated unknown coefficients needed to fit numerical results, Ergun equation may be compared with simulation data. Consequently, the Ergun curve

https://doi.org/10.4208/cicp.191114.270315a Published online by Cambridge University Press

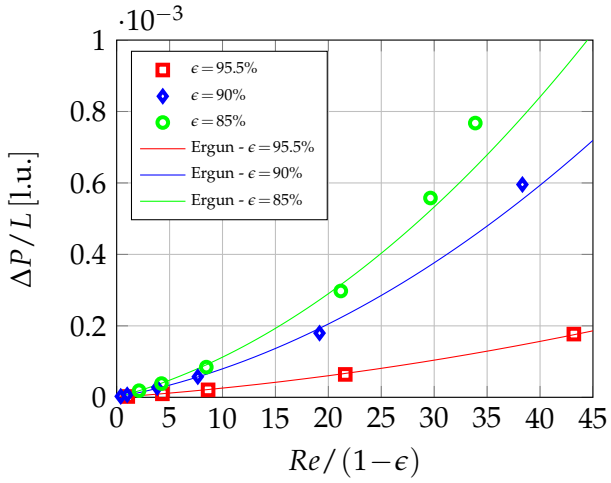


Figure 7: Numerical simulations results and Ergun equation comparison.

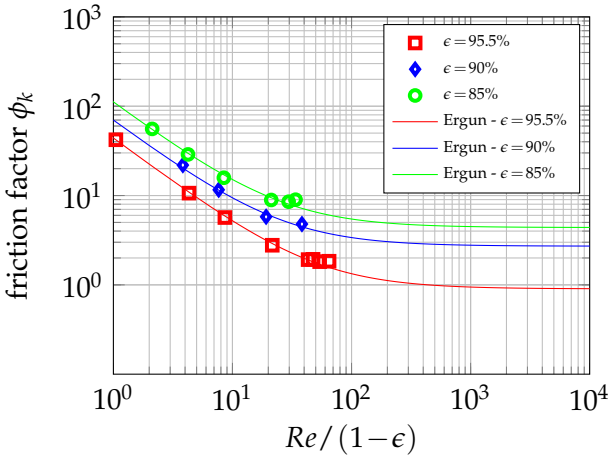


Figure 8: Numerical simulations results and Ergun equation comparison in a log-log diagram.

may be used in order to predict porous media behaviour for higher particle Reynolds numbers. In Fig. 7, the comparison between numerical simulations and Ergun curve is depicted. As it can be noticed from Fig. 7 there is a good agreement between numerical results and evaluated Ergun equations. There are some slight misalignments for 85% porosity due to high flow resistance. Nevertheless, the agreement between results is definitely acceptable.

For a large number of engineering applications, higher Reynolds numbers should be considered. At a first stage this may be carried out by means of Ergun equation prediction. Of course, some numerical or experimental validations are required too. In Fig. 8 the trend for high Reynolds numbers is shown in a log-log diagram. Looking at the previous figure, it is apparent how the asymptote for all the three curves is the B coefficient value

https://doi.org/10.4208/cicp.191114.270315a Published online by Cambridge University Press

reported in Table 6, while the first part of the curves may be represented as a constant slope line.

In order to extend the LBM simulations to a wider particle Reynolds number range a finer grid is required. Consequently, the computational requirements needed to solve the new problems have to be increased too. By the way, in this first analysis, authors want to point out benefits of coupling a random packing grid generation [9], with a single relaxation time LB approach [11, 13].

9 Conclusions

In conclusion, the coupling of an algorithm for random spheres generation [9], and a single relaxation time LBM [11] has been presented. Results have been analysed both in terms of friction factor and porosity with a good matching with experimental data presented by [10]. Moreover, both grid definition sensitivity and porosity influence have been deeply analysed in order to understand the fluid dynamics response to parameters variation. Good results have been shown in the present paper, nevertheless, the challenge is to reach higher particle Reynolds numbers which are characteristic of the interesting engineering applications.

Acknowledgments

Authors would really thank Eng. Alessandro De Maio from Nu.m.i.di.a. Srl for the always fruitful discussions fundamental for code development.

References

[1] D. P. Haack, K. R. Butcher, T. Kim, H. Hoduston, T. J. Lu, Novel Lightweight Metal Foam Heat Exchangers, Proceedings V.3 (PID-4B: Heat Exchangers Applications for Change of Phase Media and Fuel Cells Systems, Book No. I00548) (2001) 1–7.

[2] S. Mahjoob, K. Vafai, A synthesis of fluid and thermal transport models for metal foam heat exchangers, International Journal of Heat and Mass Transfer 51 (2008) 3701–3711. doi:10.1016/j.ijheatmasstransfer.2007.12.012.

[3] A. Bhattacharya, R. L. Mahajan, Finned Metal Foam Heat Sinks for Electronics Cooling in Forced Convection, Journal of Electronic Packaging 124 (3) (2002) 155–163. doi:10.1115/1.1464877.

[4] K. Boomsma, D. Poulikakos, F. Zwick, Metal foams as compact high performance heat exchangers, Mechanics of Materials 35 (2003) 1161–1176. doi:10.1016/j.mechmat.2003.02.001.

[5] C. Perrot, R. Panneton, X. Olny, Periodic unit cell reconstruction of porous media: Application to open-cell aluminum foams, Journal of Applied Physics 101 (11) (2007) 113538–11. doi:10.1063/1.2745095.

[6] R. M. Sullivan, L. J. Ghosn, B. A. Lerch, A general tetrakaidecahedron model for open-celled foams, International Journal of Solids and Structures 45 (2008) 1754–1765. doi:10.1016/j.ijsolstr.2007.10.028.

https://doi.org/10.4208/cicp.191114.270315a Published online by Cambridge University Press

[7] M. Bai, J. N. Chung, Analytical and numerical prediction of heat transfer and pressure drop in open-cell metal foams, International Journal of Thermal Sciences 50 (2011) 869–880. doi:10.1016/j.ijthermalsci.2011.01.007.
[8] P. De Jaeger, C. T'Joen, H. Huisseune, B. Ameel, M. De Paepe, An experimentally validated and parameterized periodic unit-cell reconstruction of open-cell foams, Journal of Applied Physics 109 (10) (2011) 103519–10. doi:10.1063/1.3587159.
[9] R. Al-Raoush, M. Alsaleh, Simulation of random packing of polydisperse particles, Powder Technology 176 (1) (2007) 47–55. doi:10.1016/j.powtec.2007.02.007.
[10] D. Beugre, S. Calvo, G. Dethier, M. Crine, D. Toye, P. Marchot, Lattice Boltzmann 3D flow simulations on a metallic foam, Journal of Computational and Applied Mathematics 234 (7) (2010) 2128–2134. doi:10.1016/j.cam.2009.08.100.
[11] S. Succi, The Lattice Boltzmann Equation for Fluid Dynamics and Beyond, Carendon Press - Oxford, 2001.
[12] R. Benzi, S. Succi, M. Vergassola, The lattice Boltzmann equation: theory and applications, Physics Reports 222 (1992) 145–197. doi:10.1016/0370-1573(92)90090-M.
[13] C. K. Aidun, J. R. Clausen, Lattice-Boltzmann Method for Complex Flows, Annual Review of Fluid Mechanics 42 (2010) 439–472. doi:10.1146/annurev-fluid-121108-145519.
[14] G. Falcucci, S. Ubertini, C. Biscarini, S. Di Francesco, D. Chiappini, S. Palpacelli, A. De Maio, S. Succi, Lattice Boltzmann Methods for Multiphase Flow Simulations across Scales, Communications in Computational Physics 1 (2010) 1–35. doi:10.4208/cicp.221209.250510a.
[15] G. Falcucci, S. Ubertini, D. Chiappini, S. Succi, Modern lattice Boltzmann methods for multiphase microflows, IMA Journal of Applied Mathematics 76 (5) (2011) 712–725. doi:10.1093/imamat/hxr014.
[16] S. Ergun, A. A. Orning, Fluid Flow through Randomly Packed Columns and Fluidized Beds, Industrial & Engineering Chemistry 41 (48) (1949) 1179–1184. doi:10.1021/ie50474a011.
[17] S. Chen, G. D. Doolen, Lattice Boltzmann Method for Fluid Flows, Annual Review of Fluid Mechanics 30 (1998) 329–364. doi:10.1146/annurev.fluid.30.1.329.
[18] K. Xu, X. He, Lattice Boltzmann method and gas-kinetic BGK scheme in the low-Mach number viscous flow simulations, Journal of Computational Physics 190 (190) (2003) 100–117. doi:10.1016/S0021-9991(03)00255-9.
[19] Z. Guo, T. S. Zhao, Lattice Boltzmann model for incompressible flows through porous media, Physical Review E - Statistical, Nonlinear, and Soft Matter Physics 66. doi:10.1103/PhysRevE.66.036304.
[20] F. A. L. Dullien, Porous Media: Fluid Transport and Fluid Structures, Academic Press Limited, 1992.
[21] J. Comiti, N. E. Sabiri, A. Montillet, Experimental characterization of flow regimes in various porous media - III: Limit of Darcy's or creeping flow regime for Newtonian and purely viscous non-Newtonian fluids, Chemical Engineering Science 55 (2000) 3057–3061. doi:10.1016/S0009-2509(99)00556-4.
[22] R. Al-Raoush, Extraction of physically-realistic pore network properties from three-dimensional synchrotron microtomography images of unconsolidated porous media, Ph.D. thesis (2002).

https://doi.org/10.4208/cicp.191114.270315a Published online by Cambridge University Press